In Situ Modification of a Delafossite-Type PdCoO2 Bulk Single Crystal for Reversible Hydrogen Sorption and Fast Hydrogen Evolution

Guowei Li,*,[†,#] Seunghyun Khim,[†,#] Celesta S. Chang,[∇,#] Chenguang Fu,[†] Nabhanila Nandi,[†] Fan Li,[§] Qun Yang,[†] Graeme R. Blake,[‡] Stuart Parkin,[§] Gudrun Auffermann,[†] Yan Sun,[†] David A. Muller,[∥,¶] Andrew P. Mackenzie,[†,⊥] and Claudia Felser*,[†]

[†]Max Planck Institute for Chemical Physics of Solids, 01187 Dresden, Germany
[∇]Department of Physics, Cornell University, Ithaca, New York 14853, United States
[§]Max Planck Institute for Microstructure Physics, 06120 Halle, Germany
[‡]Zernike Institute for Advanced Materials, University of Groningen, 9747 AG Groningen, The Netherlands
[∥]School of Applied and Engineering Physics, Cornell University, Ithaca, New York 14853, United States
[¶]Kavli Institute at Cornell for Nanoscale Science, Cornell University, Ithaca, New York 14853, United States
[⊥]Scottish Universities Physics Alliance, School of Physics and Astronomy, University of St. Andrews, Fife KY16 9SS, United Kingdom

S *Supporting Information*

ABSTRACT: The observation of extraordinarily high conductivity in delafossite-type $PdCoO_2$ is of great current interest, and there is some evidence that electrons behave like a fluid when flowing in bulk crystals of $PdCoO_2$. Thus, this material is an ideal platform for the study of the electron transfer processes in heterogeneous reactions. Here, we report the use of bulk single-crystal $PdCoO_2$ as a promising electrocatalyst for hydrogen evolution reactions (HERs). An overpotential of only 31 mV results in a current density of 10 mA cm^{-2}, accompanied by high long-term stability. We have precisely determined that the crystal surface structure is modified after electrochemical activation with the formation of strained Pd nanoclusters in the surface layer. These nanoclusters exhibit reversible hydrogen sorption and desorption, creating more active sites for hydrogen access. The bulk $PdCoO_2$ single crystal with ultrahigh conductivity, which acts as a natural substrate for the Pd nanoclusters, provides a high-speed channel for electron transfer.
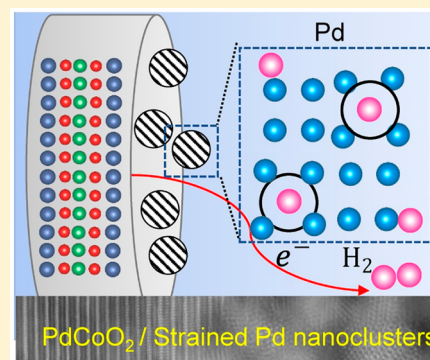
Delafossite-type metals such as $PdCoO_2$ are currently attracting considerable attention due to their exotic and surprising physical properties. The most striking characteristic is their remarkably low electrical resistivity, lower than those of all normal state oxides yet reported.[1−3] Pd 4d states contribute to the density of states at the Fermi level with sp band-like fast dispersion.[4,5] This leads to an ultrahigh carrier velocity of ∼4.96 × 10^5 m/s, which even approaches that of graphene with a velocity on the order of ∼10^6 m/s.[1,6−8] Of particular interest is the observation of hydrodynamic electron flow in bulk $PdCoO_2$ single crystals, suggesting the anomalous suppression of momentum relaxation resulting from electron impurity and electron−electron and electron−phonon interactions.[9] In addition, $PdCoO_2$ exhibits a strong quasi-two-dimensional nature, characterized by higher in-plane conductivity than that along the normal direction. This represents an ideal research prototype to study the relationship between conductivity and surface reactions, especially in the field of electrochemistry.

Hydrogen production from electrochemical water splitting does not only have potential to face the challenge of global environmental and energy problems but also serves as a model for the study of other complex heterogeneous catalysis reactions.[10−15] It is commonly agreed that an ideal electro-
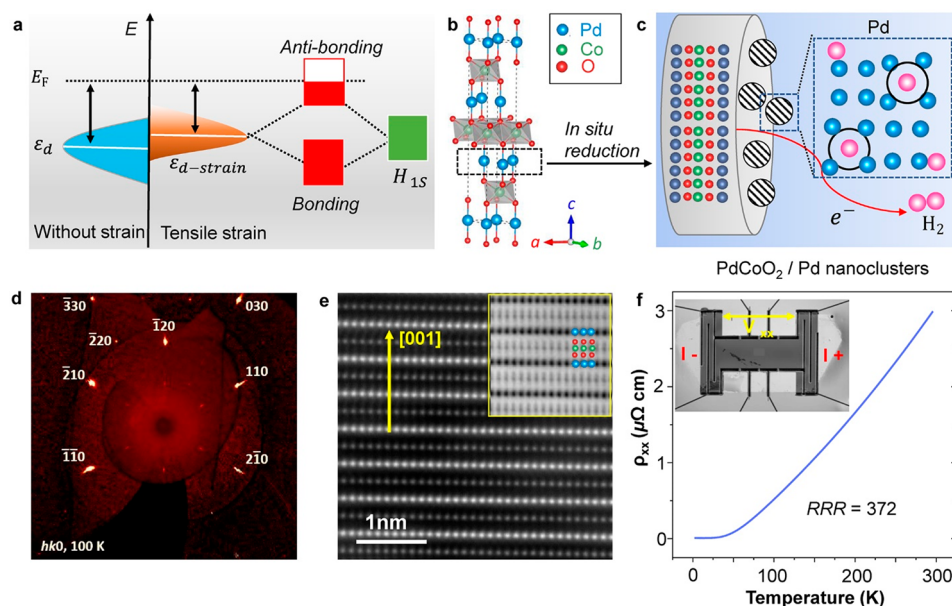
Figure 1. (a) Changes in d bands at the transition metal surface in the presence of tensile strain. A shift of the d-band center is expected when coupled with H adsorbates. (b) Crystal structure of a $PdCoO_2$ single crystal obtained by single-crystal XRD. (c) Hydrogen adsorption/absorption process and electron transfer process on the in situ modified $PdCoO_2$ single-crystal surface. Pink spheres are hydrogen atoms, and blue spheres are Pd atoms. (d) Single-crystal XRD precession image of the $hk0$ reciprocal space plane of a bulk $PdCoO_2$ crystal. (e) HADDF-STEM image showing the cross section of the $PdCoO_2$ single crystal [120] prepared by FIB. The inset shows an ABF-STEM image, resolving the oxygens clearly. The crystal structure is overlaid, where Pd, Co, and O atoms are represented by blue, green, and red circles, respectively. (f) Temperature-dependent electrical resistivity of the single crystal measured using a device fabricated by FIB, as shown in the inset.

catalyst for hydrogen evolution reaction (HER) has a large exchange current density, a low Tafel slope, and high electrochemical stability. The efficiency of a given catalyst is mainly determined by the first two factors, which in turn represent electron transfer barriers. Further investigation of the HER process revealed that two electron transfer processes are involved. The first one involves electron transfer from the catalyst surface to the reaction intermediate. This is governed by the Sabatier principle based on the d-band model, which states that an optimal binding energy of the intermediate will favor the reaction. The second process is the injection of electrons from the substrate (e.g., glassy carbon electrode) to the catalyst and then flow to the surface.

We can now ask two interesting questions. What is the HER performance of a bulk single crystal with strikingly low room-temperature resistivity? Can we combine the characteristics of high current density, low Tafel slope and high electrochemical stability in a single compound?

Herein, we report the synthesis of high-quality $PdCoO_2$ single crystals such that we can observe their high-conductivity (001) crystal surface. Serving as both an electrode and catalyst for HER, $PdCoO_2$ exhibits remarkable electrocatalytic activity with an extremely low overpotential, low Tafel slope, and good stability, outperforming the state-of-the-art Pt catalyst. Scanning transmission electron microscopy (STEM) revealed the nature of the precise surface modification process in the catalytic environment. The formation of a surface layer consisting of Pd nanoclusters and cobalt oxide is responsible for the high activity with respect to HER. We observe reversible hydrogen sorption and desorption in these Pd nanoclusters, which formed in situ on the bulk $PdCoO_2$ single-crystal surface. This provides a large number of active sites for hydrogen access. The bulk single-crystal substrate also served

as an expressway for electron transfer. Our findings suggest that the in situ modification of a high-conductivity bulk single crystal is crucial for tuning its electrocatalytic activity.

Let us first summarize our strategy and its advantages. For HER catalysts, it has been confirmed that the surface reactivity trends can be rationalized by the d-band theory (Figure 1a). The chemisorption of H on transition metals results in coupling between the H 1s band and the metal d bands. The average energy of the electronic d states projected onto a surface metal atom (the d-band center ε_d) determines the filling of adsorbate–metal antibonding states and further controls the activity. However, once strain is introduced in the transition metal, the interatomic bond lengths and the environment can change. For transition metals with more than half-filled d bands, a tensile strain should upshift the d-band center to preserve the degree of d-band filling.[16,17] Generally, strain can be introduced either by preparing nanostructures or by depositing on the substrate with mismatched crystal lattices, where one can observe the strain at the interface, within the facets, or at the edges of the catalyst. Unfortunately, these strategies generally result in an uncertain distribution and extent of strain. $PdCoO_2$ adopts a quasi-two-dimensional structure, with Co atoms forming distorted octahedra with oxygen atoms, and are interlinked by single Pd layers along the c axis.[2] As a cathode material for HER, we expect in situ formation of Pd nanoclusters during the reduction process (Figure 1b). Such a layer-by-layer growth process at the expense of $PdCoO_2$ may introduce strain not only confined to the crystal surface but also in the bulk. The formation of Pd nanoclusters is extremely important for hydrogen adsorption and absorption in the subsequent hydrogen reduction process (Figure 1c).

Single crystals of PdCoO₂ were grown via a reaction between stoichiometric amounts of PdCl₂ and CoO.[9,18] A typical single crystal is displayed in Figure S1, showing metallic luster and well-defined steps typical of a layered structure. The atomic stoichiometries of Co, Pd, and O are determined to be approximately 1:1:2 for both the surface and the sides (Figure S2), indicating high homogeneity of the bulk single crystal. More accurately, de Haas−van Alphen measurements of the Fermi volume confirm stoichiometry to within the ∼1% accuracy of that technique.[8] The high purity of the sample is confirmed by the X-ray diffraction (XRD) pattern recorded on the powder crushed from a bulk single crystal (Figure S3). All of the diffraction peaks can be indexed to PdCoO₂ with space group $R\bar{3}m$ (space group no. 166). More details are given by single-crystal XRD at 100 and 295 K (Figure 1b). PdCoO₂ crystallizes in the hexagonal system with space group $R\bar{3}m$ and lattice parameters of $a = b = 0.2845(3)$ nm and $c = 1.7880(14)$ nm at 295 K. The crystal is highly layered, leading to some smearing and splitting of spots in the stacking direction (see the $0kl$ reciprocal lattice plane in Figure S4), probably caused by slight rotations of the layers along the stacking direction. In contrast, the degree of in-plane order is very good, as can be seen by the sharp spots in the $hk0$ reciprocal lattice plane (Figure 1d). A cross-sectional TEM lamella was prepared from the as-grown single crystal using a focused ion beam (FIB) (Figure S5). The lattice structure clearly shown in the enlarged STEM image shows the high crystallinity of the PdCoO₂ crystal (Figure 1e). The high-angle annular dark-field (HAADF-STEM) image emphasizes the repeating layers of Pd and CoO; the inset annular bright-field (ABF-STEM) image also shows the oxygen atoms in the CoO layer. The HAADF-STEM image that looks down on the [001] crystal zone proved the exposure of the (001) crystal surface (Figure S6). The surface composition and electronic structure were investigated by X-ray photoelectron spectroscopy (Figure S7). The prominent Pd $3d_{5/2}$ peak at 335.4 eV is assigned to the Pd−O bonds in PdCoO₂ (Figure S8). This binding energy is slightly larger than that of pure Pd (334.8- 335.1 eV) but significantly lower than that in PdO.[19,20] This indicates that Pd adopts the monovalent state in the PdCoO₂ crystal. Thus, the Pd−O layer should be a good metal from the viewpoint of the ionic picture, which is further confirmed by the asymmetric shape of the peak and the plasmonic energy loss feature.[7] Extensive photoemission studies of surface states have quantified the level of charge redistribution at Co−O-terminated[21] and Pd-terminated[22] surfaces of bulk crystals.

In this study, the same PdCoO₂ bulk single crystals were used as both the cathode and electrocatalyst. Thus, their electrical conductivity is extremely important for the HER activity. Devices with well-defined geometry were fabricated by FIB sculpting, as shown in the inset of Figure 1f. The temperature dependence of the resistivity exhibits the behavior of a metal. The room-temperature resistivity was only 2.9 $\mu\Omega$ cm, one of the lowest electrical resistivities among all reported metal oxides. This value is even lower than those of benchmark metal catalysts such as Pt (10.6 $\mu\Omega$ cm), Pd (10.5 $\mu\Omega$ cm), Ru (7.1 $\mu\Omega$ cm), and Ir (4.7 $\mu\Omega$ cm). The residual resistivity ratio (RRR), $R(300K)/R(2K)$, is 372, indicating the high quality of the bulk crystal.

The well-defined exposed crystal surface, as well as the ultrahigh room-temperature conductivity, makes the crystal suitable for studying the surface HER mechanism. The electrochemical characteristics of the bulk single crystal were

measured using a standard three-electrode setup in 0.5 M H₂SO₄(aq). The iR-corrected polarization curves of PdCoO₂ and a 20% Pt/C catalyst are shown in Figure 2a. To achieve a
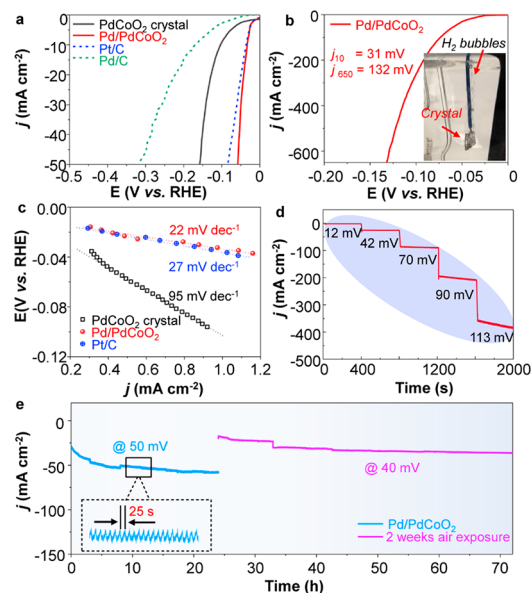
Figure 2. (a) Polarization curves of the modified bulk PdCoO₂ single crystal and 20% Pt/C, Pd/C commercial catalysts. (b) Polarization curves of the bulk PdCoO₂ single crystal at larger applied overpotential. The inset shows the produced hydrogen bubbles on the crystal surface. (c) Tafel plots of the bulk PdCoO₂ single crystal catalysts and 20% Pt/C catalyst. (d) Multicurrent process showing the current density increasing from 5 to 350 mA cm⁻² without iR correction. (e) Current versus time over 24 h showing a constant potential of −50 mV, which is reduced to −40 mV (for 48 h) after 2 weeks of exposure to air.

catalytic current density of 10 mA cm⁻², the modified PdCoO₂ single crystal requires an overpotential of 31 mV, which is even lower than that of commercial Pt/C (35 mV). More strikingly, a very small overpotential of only 132 mV was needed to deliver a current density of 650 mA cm⁻² (Figure 2b). Hydrogen bubbles are produced furiously on the crustal surface (inset of Figure 2b). To the best of our knowledge, this represents one of the best electrocatalysts with such high HER activity (Table S1).[23−32] Tafel slopes of 22 and 27 mV dec⁻¹ were obtained for the modfied PdCoO₂ single crystal and Pt/C catalyst from the Tafel plots (Figure 2c). This suggests that the Tafel recombination step is the rate-determining step and is responsible for the particularly high activity of single-crystal PdCoO₂, similar to the benchmark Pt catalyst,[33−36] The rapid response of the current density to voltage, as obtained from the multiple-step chronopotentiometry experiments, revealed the high mass transport and mechanical robustness of the single crystal (Figure 2d).

The single-crystal catalyst also exhibited outstanding long-term operational stability over 24 h at a constant overpotential (Figure 2e). By magnifying the catalytic current density versus time plot, a wave mode signal was observed, originating from the rapid hydrogen bubble release (inset of Figure 2e). Remarkably, after exposing the same crystal to air for 2 weeks, it still shows high stability beyond 48 h. Finally, the amount of H₂ gas produced was collected at a HER current of 4 mA. A comparison with the theoretical value revealed a Faradaic efficiency of ∼100% (Figure S9).

Next, we will attempt to understand the origin of the high HER activity of the PdCoO$_2$ single crystal. The experiment was repeated using two fresh crystals, showing similar behavior, as discussed below. Specifically, the fresh crystals did not show such impressive activity in the initial test (Figure 2a). A much larger overpotential of 105 mV was needed to achieve a current density of 10 mA cm^{-2}, accompanied by a steeper Tafel slope of 95 mV dec^{-1} (Figure 2a,c). This may explain why delafossite PdCoO$_2$ has not received much attention as a HER catalyst. The activation process can be further elucidated by the stability test (Figure 2e). At an overpotential of ~50 mV, the catalytic current density increases continuously with time. Thus, we conclude that the surface of fresh single-crystal PdCoO$_2$ must be reconstructed and optimized to favor HER kinetics.

A SEM image of a fresh crystal reveals a smooth and flat surface (Figure 3a). In contrast, many coniform islands are
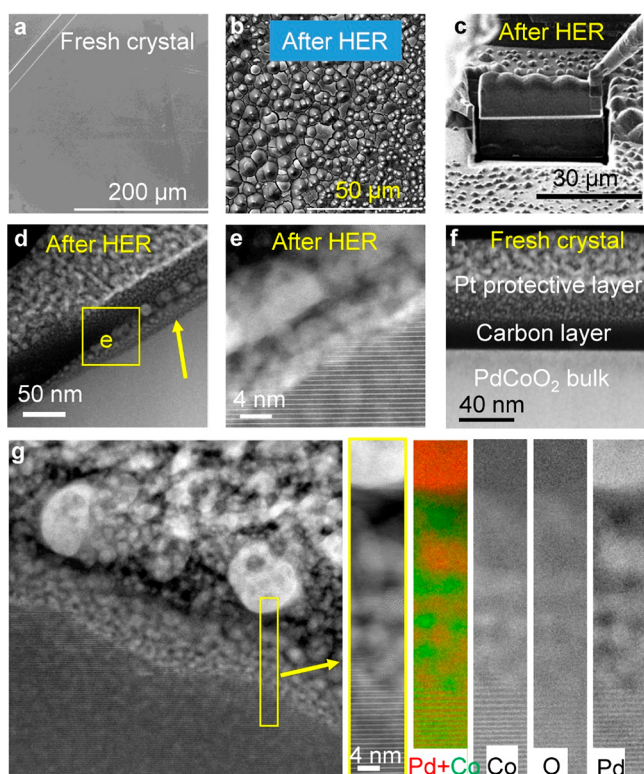

Figure 3. (a) SEM image of a fresh PdCoO$_2$ single-crystal surface. (b) SEM image of the crystal surface after HER. (c) A thin lamella including three islands is cut out by FIB. (d) HAADF-STEM image of the single-crystal surface after HER. A new surface layer is observed, as indicated by the yellow arrow. (e) Magnified STEM image of the interface indicated by the square in (d). (f) HAADF-STEM image of a fresh single-crystal surface before HER. Compared to (d) and (e), there are no surface layers. (g) EELS elemental mapping across the interface. Pd and Co are clearly separated. O is detected only in the area where Co is present. We thus conclude that Pd nanoclusters and cobalt oxides are formed in the surface layer.

observed after HER measurement (Figure 3b). To elucidate the detailed structure of these islands, a cross-sectional TEM lamella showing these features was fabricated using a FIB for TEM analysis (Figures 3c and S10 and 11). A comparison of the TEM images of a fresh crystal (Figure 3f) and an activated crystal (Figure 3d) indicate that in the activated crystal a new surface layer of up to tens of nanometers is observed, as

pointed out by the yellow arrow. Magnified STEM images of this area are shown in Figure 3e,g, where numerous polycrystalline Pd nanoparticles and cobalt oxide inclusions are observed in the new layer with distinctly different lattice structures from bulk PdCoO$_2$. Electron energy loss (EELS) chemical mapping was performed carefully across the interface (Figures 3g and S12). The bright spots in the oxygen map overlap exactly with the Co signal in the cobalt map, whereas there is no Pd signal corresponding to these regions. The elemental color mapping further confirms that the newly formed surface layer contains large polycrystalline Pd clusters at the top, followed by an intermediate layer comprising small Pd nanoclusters and cobalt oxide inclusions, with the PdCoO$_2$ bulk crystal at the bottom showing clearly distinguishable periodic Pd and CoO layers. From the multivariate curve resolution (MCR) processing of the resolved EELS spectra, we observe a slight shift of the Co spectrum peak from the nanoparticle layer with respect to that from the bulk PdCoO$_2$. We determined that the cobalt in the surface layer is in the Co^{2+} valence state by comparing the obtained cobalt L$_{2,3}$-edge EELS spectrum with a reference spectrum (Figure S13).

We studied the HER activities of various reported Pd and CoO structures (Table S2) and concluded that activity as impressive as that obtained herein has never been achieved before, especially with CoO phase catalysts. This suggests that the in situ formation of a surface layer comprising Pd nanoclusters is closely related to the remarkable HER activity of bulk PdCoO$_2$ crystals. Cyclic voltammetry (CV) was next used to understand the hydrogen adsorption and absorption behavior on the crystal surface. Figure 4a shows that the cathodic and anodic peaks between 0.25 and 0.4 V correspond
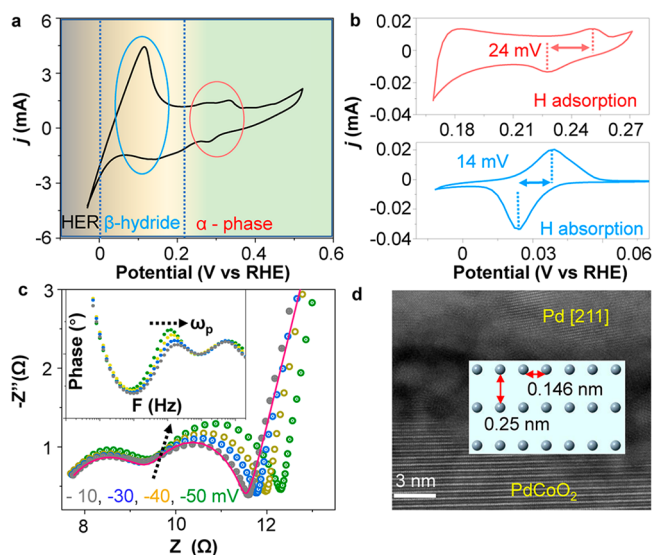

Figure 4. (a) CV curve of a PdCoO$_2$ single crystal at a scan rate of 20 mV/s. The formations of various phases in different potential ranges are separated by dotted lines. (b) CV curves recorded in the hydrogen adsorption and absorption range at a scan rate of 1 mV/s, corresponding to the formation of the α-phase and β-phase, respectively. (c) Nyquist plots of the PdCoO$_2$ single crystal with different overpotentials. The corresponding Bode phase plots are shown in the inset. (d) HAADF-STEM image of the surface modified PdCoO$_2$ single crystal. The measured apparent spacings between Pd atoms on the (211) projection of a Pd nanocluster are 0.25 and 0.146 nm, which are significantly larger than the corresponding distances for pure Pd.

to hydrogen adsorption and formation of the α-phase (Pd + H) at the Pd nanocrystal surface. The formation of the β-phase hydride (PdH$_x$) is observed at a low potential and saturates at ~0 mV. This is followed by the hydrogen evolution process when the potential vs RHE is negative. These features are in good agreement with previous results obtained using various Pd structures.[37] To achieve full saturation of hydrogen at the crystal surface, a much slower scan rate of 1 mV/s was used. The corresponding CV curves (Figure 4b) provide two important results. First, the hydrogen adsorption/desorption and absorption/desorption charges are almost the same during the potential scans. Second, the potential hysteresis between the adsorption and absorption processes are only 24 and 14 mV, significantly lower than those obtained for Pd nanoparticles of the same size and other Pd structures. Because the hysteresis reflects electrochemical reversibility of the hydrogen absorption/desorption processes, this implies high reversibility in the present system.[38]

Electrochemical impedance spectroscopy (EIS) was used to investigate the electron transfer and hydrogen sorption mechanisms. The EIS patterns at different potentials were recorded in the overpotential deposition (OPD) region, corresponding to the HER process (Figure 4c). The patterns can be fitted by a two-time constant serial (2TS) model, with two semicircles observed in the Nyquist plots (Figure S14). The semicircle at high frequency (HF), which is strongly independent of the overpotential, can be assigned to electron transfer from the electrode to the catalyst.[39,40] More specifically, this corresponds to electron transfer from the bulk PdCoO$_2$ single crystal to the surface Pd nanoparticles. The low frequency (LF) semicircle depends on the overpotentials. This is related to the charge transfer kinetics in the HER process, corresponding to a faster reaction rate. The Bode phase diagram reveals two relaxation times (Figures 4c and S15). With increasing overpotential, the intensity of the LF semicircle decreases and shifts to a higher frequency, indicating an increase in the reaction rate and a shorter reaction time constant ($\tau = 1/\omega_p$, where τ is the time constant and ω_p is the characteristic frequency).[41,42] In contrast, the time constant at HF has a slight decrease in density and is much lower than the HER kinetics value. This corresponds to the response of a fast electron transfer process, as proposed by Omanovic et al.[43] Thus, we can conclude that the high electrical conductivity of the PdCoO$_2$ single crystal is of great importance for electron injection onto the catalyst surface.

The formation of the β-phase PdH$_x$ as a result of hydrogen sorption also leads to another phenomenon. Figure 4d shows that the average apparent distances between Pd atoms in the (211) plane projection of the Pd nanoclusters are 0.25 and 0.16 nm, which are significantly larger than the corresponding distances in pure Pd (0.25 and 0.137 nm) (more details in Figure S16). This corresponds to anisotropic tensile strains of 10 and 6.2% along the longer and shorter lengths of Pd, respectively. The volcano plot obtained based on the Sabatier principle suggests that the adsorption energies of reaction intermediates are always very high on transition metal surfaces, leading to sluggish HER kinetics.[44,45] The introduction of strain on the catalyst surface has been proven as an effective strategy to regulate the adsorbate energies.[46] A shift of the d-band center was observed for various transition metals including Pd, Pt, Ir, Ni, and Co, when the strain was created, regardless of the exposed catalyst surface.[47] Indeed, our calculations suggests an up-shift of the d-band center from

−2.30 eV for the pristine sample to −2.19 eV after applying a tensile strain (Figure S17). An attractive point of our current study is, rather than following strategies like creating defects, alloying, and depositing on a substrate with different lattice constants, that strain is introduced in situ during the HER process on the highly conducive PdCoO$_2$ single-crystal surface.[44,48,49] Problems like mechanical instability, strain relaxation, discontinuous strain distribution, and dissolution can be avoided by this method.

In summary, high-quality bulk single crystals of PdCoO$_2$ have been synthesized and their electrochemical HER behavior has been studied systematically. We observe reconstruction of the crystal surface, leading to the in situ formation of a surface layer comprising Pd nanoclusters and cobalt oxide. It is demonstrated that these Pd nanoclusters exhibit high hydrogen sorption/desorption reversibility, which creates more active sites for hydrogen to access during the subsequent HER process. In addition, the ultrahigh conductivity of the PdCoO$_2$ single-crystal substrate provides an expressway for electron injection into the catalyst surface. The methodology presented herein provides a general way for in situ modification and fabrication of high-efficiency HER electrocatalysts.

■ ASSOCIATED CONTENT

Ⓢ Supporting Information

The Supporting Information is available free of charge on the ACS Publications website at DOI: 10.1021/acsenergylett.9b01527.

> Experimental methods, SEM images, EDS spectra, HAADF-STEM images, XPS spectra, STEM-EDS mapping, LEIS spectrum, EIS spectra, and HER activity tables (PDF)

> Crystallographic data for PdCoO2_295K (CIF)

■ AUTHOR INFORMATION

Corresponding Authors
*E-mail: Guowei.li@cpfs.mpg.de.
*E-mail: Claudia.felser@cpfs.mpg.de.

ORCID Ⓘ
Guowei Li: 0000-0003-1837-3967
Seunghyun Khim: 0000-0002-9495-7406
Chenguang Fu: 0000-0002-9545-3277
Graeme R. Blake: 0000-0001-9531-7649

Author Contributions
#G.L, S.K., and C.S.C. contributed equally to this work.

Notes
The authors declare no competing financial interest.
The research data supporting this publication can be accessed at https://doi.org/10.17630/4f818aaa-e937-46e6-9257-161689cdf399.

■ REFERENCES

(1) Mackenzie, A. P. The properties of ultrapure delafossite metals. *Rep. Prog. Phys.* **2017**, *80* (3), 032501.

(2) Eyert, V.; Fresard, R.; Maignan, A. On the metallic conductivity of the delafossites PdCoO$_2$ and PtCoO$_2$. *Chem. Mater.* **2008**, *20* (6), 2370−2373.

(3) Nandi, N.; Scaffidi, T.; Kushwaha, P.; Khim, S.; Barber, M. E.; Sunko, V.; Mazzola, F.; King, P. D. C.; Rosner, H.; Moll, P. J. W.; König, M.; Moore, J. E.; Hartnoll, S.; Mackenzie, A. P. Unconventional magneto-transport in ultrapure PdCoO$_2$ and PtCoO$_2$. *npj Quant. Mater.* **2018**, *3*, 66.

(4) Kim, K.; Choi, H. C.; Min, B. I. Fermi surface and surface electronic structure of delafossite PdCoO$_2$. *Phys. Rev. B: Condens. Matter Mater. Phys.* **2009**, *80* (3), 035116.

(5) Usui, H.; Ochi, M.; Kitamura, S.; Oka, T.; Ogura, D.; Rosner, H.; Haverkort, M. W.; Sunko, V.; King, P. D. C.; Mackenzie, A. P.; Kuroki, K. Hidden kagome-lattice picture and origin of high conductivity in delafossite PtCoO$_2$. *Phys. Rev. Mater.* **2019**, *3* (4), 045002.

(6) Nair, R. R.; Tsai, I. L.; Sepioni, M.; Lehtinen, O.; Keinonen, J.; Krasheninnikov, A. V.; Castro Neto, A. H.; Katsnelson, M. I.; Geim, A. K.; Grigorieva, I. V. Dual origin of defect magnetism in graphene and its reversible switching by molecular doping. *Nat. Commun.* **2013**, *4*, 2010.

(7) Noh, H. J.; Jeong, J.; Jeong, J.; Cho, E. J.; Kim, S. B.; Kim, K.; Min, B. I.; Kim, H. D. Anisotropic electric conductivity of delafossite PdCoO$_2$ studied by angle-resolved photoemission spectroscopy. *Phys. Rev. Lett.* **2009**, *102* (25), 256404.

(8) Hicks, C. W.; Gibbs, A. S.; Mackenzie, A. P.; Takatsu, H.; Maeno, Y.; Yelland, E. A. Quantum oscillations and high carrier mobility in the delafossite PdCoO$_2$. *Phys. Rev. Lett.* **2012**, *109* (11), 116401.

(9) Moll, P. J. W.; Kushwaha, P.; Nandi, N.; Schmidt, B.; Mackenzie, A. P. Evidence for hydrodynamic electron flow in PdCoO$_2$. *Science* **2016**, *351* (6277), 1061−1064.

(10) Peng, J.; Chen, X.; Ong, W.-J.; Zhao, X.; Li, N. Surface and Heterointerface Engineering of 2D MXenes and Their Nanocomposites: Insights into Electro- and Photocatalysis. *Chem.* **2019**, *5* (1), 18−50.

(11) Csernica, P. M.; McKone, J. R.; Mulzer, C. R.; Dichtel, W. R.; Abruña, H. D.; DiSalvo, F. J. Electrochemical Hydrogen Evolution at Ordered Mo$_7$Ni$_7$. *ACS Catal.* **2017**, *7* (5), 3375−3383.

(12) Rizo, R.; Aran-Ais, R. M.; Padgett, E.; Muller, D. A.; Lazaro, M. J.; Solla-Gullon, J.; Feliu, J. M.; Pastor, E.; Abruna, H. D. Pt-Richcore/Sn-Richsubsurface/Ptskin Nanocubes As Highly Active and Stable Electrocatalysts for the Ethanol Oxidation Reaction. *J. Am. Chem. Soc.* **2018**, *140* (10), 3791−3797.

(13) Liu, Y.; Xiao, C.; Huang, P.; Cheng, M.; Xie, Y. Regulating the Charge and Spin Ordering of Two-Dimensional Ultrathin Solids for Electrocatalytic Water Splitting. *Chem.* **2018**, *4* (6), 1263−1283.

(14) Yuan, Z.; Bak, S.-M.; Li, P.; Jia, Y.; Zheng, L.; Zhou, Y.; Bai, L.; Hu, E.; Yang, X.-Q.; Cai, Z.; Sun, Y.; Sun, X. Activating Layered Double Hydroxide with Multivacancies by Memory Effect for Energy-Efficient Hydrogen Production at Neutral pH. *ACS Energy Lett.* **2019**, *4* (6), 1412−1418.

(15) Jin, S. Are Metal Chalcogenides, Nitrides, and Phosphides Oxygen Evolution Catalysts or Bifunctional Catalysts? *ACS Energy Lett.* **2017**, *2* (8), 1937−1938.

(16) Schnur, S.; Groß, A. Strain and coordination effects in the adsorption properties of early transition metals: A density-functional theory study. *Phys. Rev. B: Condens. Matter Mater. Phys.* **2010**, *81* (3), 033402.

(17) Luo, M.; Guo, S. Strain-controlled electrocatalysis on multimetallic nanomaterials. *Nat. Rev. Mater.* **2017**, *2* (11), 17059.

(18) Shannon, R. D.; Rogers, D. B.; Prewitt, C. T. Chemistry of noble metal oxides. I. Syntheses and properties of ABO$_2$ delafossite compounds. *Inorg. Chem.* **1971**, *10* (4), 713−718.

(19) Haack, L. P.; Otto, K. X-ray photoelectron spectroscopy of Pd/γ-aluminaand Pd foil after catalytic methane oxidation. *Catal. Lett.* **1995**, *34*, 31−40.

(20) Paredis, K.; Ono, L. K.; Behafarid, F.; Zhang, Z.; Yang, J. C.; Frenkel, A. I.; Cuenya, B. R. Evolution of the structure and chemical state of Pd nanoparticles during the in situ catalytic reduction of NO with H2. *J. Am. Chem. Soc.* **2011**, *133* (34), 13455−64.

(21) Sunko, V.; Rosner, H.; Kushwaha, P.; Khim, S.; Mazzola, F.; Bawden, L.; Clark, O. J.; Riley, J. M.; Kasinathan, D.; Haverkort, M. W.; Kim, T. K.; Hoesch, M.; Fujii, J.; Vobornik, I.; Mackenzie, A. P.; King, P. D. C. Maximal Rashba-like spin splitting via kinetic-energy-coupled inversion-symmetry breaking. *Nature* **2017**, *549* (7673), 492−496.

(22) Mazzola, F.; Sunko, V.; Khim, S.; Rosner, H.; Kushwaha, P.; Clark, O. J.; Bawden, L.; Markovic, I.; Kim, T. K.; Hoesch, M.; Mackenzie, A. P.; King, P. D. C. Itinerant ferromagnetism of the Pd-terminated polar surface of PdCoO$_2$. *Proc. Natl. Acad. Sci. U. S. A.* **2018**, *115* (51), 12956−12960.

(23) Mahmood, J.; Li, F.; Jung, S. M.; Okyay, M. S.; Ahmad, I.; Kim, S. J.; Park, N.; Jeong, H. Y.; Baek, J. B. An efficient and pH-universal ruthenium-based catalyst for the hydrogen evolution reaction. *Nat. Nanotechnol.* **2017**, *12* (5), 441−446.

(24) Kibsgaard, J.; Jaramillo, T. F.; Besenbacher, F. Building an appropriate active-site motif into a hydrogen-evolution catalyst with thiomolybdate [Mo$_3$S$_{13}$]$^{2-}$ clusters. *Nat. Chem.* **2014**, *6* (3), 248−253.

(25) Caban-Acevedo, M.; Stone, M. L.; Schmidt, J. R.; Thomas, J. G.; Ding, Q.; Chang, H. C.; Tsai, M. L.; He, J. H.; Jin, S. Efficient hydrogen evolution catalysis using ternary pyrite-type cobalt phosphosulphide. *Nat. Mater.* **2015**, *14* (12), 1245−51.

(26) Skúlason, E.; Tripkovic, V.; Björketun, M. E.; Gudmundsdóttir, S.; Karlberg, G.; Rossmeisl, J.; Bligaard, T.; Jónsson, H.; Nørskov, J. K. Modeling the Electrochemical Hydrogen Oxidation and Evolution Reactions on the Basis of Density Functional Theory Calculations. *J. Phys. Chem. C* **2010**, *114* (42), 18182−18197.

(27) Lv, H.; Xi, Z.; Chen, Z.; Guo, S.; Yu, Y.; Zhu, W.; Li, Q.; Zhang, X.; Pan, M.; Lu, G.; Mu, S.; Sun, S. A New Core/Shell NiAu/Au Nanoparticle Catalyst with Pt-like Activity for Hydrogen Evolution Reaction. *J. Am. Chem. Soc.* **2015**, *137* (18), 5859−62.

(28) Pu, Z.; Amiinu, I. S.; Kou, Z.; Li, W.; Mu, S. RuP$_2$-Based Catalysts with Platinum-like Activity and Higher Durability for the Hydrogen Evolution Reaction at All pH Values. *Angew. Chem.* **2017**, *129*, 11717−11722.

(29) Zhao, Z.; Liu, H.; Gao, W.; Xue, W.; Liu, Z.; Huang, J.; Pan, X.; Huang, Y. Surface-Engineered PtNi-O Nanostructure with Record-High Performance for Electrocatalytic Hydrogen Evolution Reaction. *J. Am. Chem. Soc.* **2018**, *140* (29), 9046−9050.

(30) Luo, Z.; Ouyang, Y.; Zhang, H.; Xiao, M.; Ge, J.; Jiang, Z.; Wang, J.; Tang, D.; Cao, X.; Liu, C.; Xing, W. Chemically activating MoS$_2$ via spontaneous atomic palladium interfacial doping towards efficient hydrogen evolution. *Nat. Commun.* **2018**, *9* (1), 2120.

(31) Li, Y.; Hasin, P.; Wu, Y. Ni$_x$Co$_{3-x}$O$_4$ nanowire arrays for electrocatalytic oxygen evolution. *Adv. Mater.* **2010**, *22* (17), 1926−1929.

(32) Pu, Z.; Amiinu, I. S.; Kou, Z.; Li, W.; Mu, S. RuP$_2$ -Based Catalysts with Platinum-like Activity and Higher Durability for the Hydrogen Evolution Reaction at All pH Values. *Angew. Chem., Int. Ed.* **2017**, *56* (38), 11559−11564.

(33) Zhang, J.; Wang, T.; Liu, P.; Liao, Z.; Liu, S.; Zhuang, X.; Chen, M.; Zschech, E.; Feng, X. Efficient hydrogen production on MoNi4 electrocatalysts with fast water dissociation kinetics. *Nat. Commun.* **2017**, *8*, 15437.

(34) Gao, M. R.; Chan, M. K.; Sun, Y. Edge-terminated molybdenum disulfide with a 9.4-Å interlayer spacing for electrochemical hydrogen production. *Nat. Commun.* **2015**, *6*, 7493.

(35) Zhang, R.; Wang, X.; Yu, S.; Wen, T.; Zhu, X.; Yang, F.; Sun, X.; Wang, X.; Hu, W. Ternary NiCo$_2$P$_x$ Nanowires as pH-Universal Electrocatalysts for Highly Efficient Hydrogen Evolution Reaction. *Adv. Mater.* **2017**, *29* (9), 1605502.

(36) Yao, R.-Q.; Zhou, Y.-T.; Shi, H.; Zhang, Q.-H.; Gu, L.; Wen, Z.; Lang, X.-Y.; Jiang, Q. Nanoporous Palladium—Silver Surface Alloys as Efficient and pH-Universal Catalysts for the Hydrogen Evolution Reaction. *ACS Energy Lett.* **2019**, *4* (6), 1379−1386.

(37) Bastide, S.; Zlotea, C.; Laurent, M.; Latroche, M.; Cachet-Vivier, C. Direct assessment from cyclic voltammetry of size effect on the hydrogen sorption properties of Pd nanoparticle/carbon hybrids. *J. Electrochem. Chem.* **2013**, *706*, 33−39.

(38) Hubkowska, K.; Soszko, M.; Symonowicz, M.; Łukaszewski, M.; Czerwiński, A. Electrochemical Behavior of a Pd Thin Film Electrode in Concentrated Alkaline Media. *Electrocatalysis* **2017**, *8* (4), 295−300.

(39) Downes, C. A.; Marinescu, S. C. Understanding Variability in the Hydrogen Evolution Activity of a Cobalt Anthracenetetrathiolate Coordination Polymer. *ACS Catal.* **2017**, *7* (12), 8605−8612.

(40) Vrubel, H.; Moehl, T.; Gratzel, M.; Hu, X. Revealing and accelerating slow electron transport in amorphous molybdenum sulphide particles for hydrogen evolution reaction. *Chem. Commun.* **2013**, *49* (79), 8985−7.

(41) Liao, L.; Wang, S.; Xiao, J.; Bian, X.; Zhang, Y.; Scanlon, M. D.; Hu, X.; Tang, Y.; Liu, B.; Girault, H. H. A nanoporous molybdenum carbide nanowire as an electrocatalyst for hydrogen evolution reaction. *Energy Environ. Sci.* **2014**, *7* (1), 387−392.

(42) Singh, R. K.; Ramesh, R.; Devivaraprasad, R.; Chakraborty, A.; Neergat, M. Hydrogen Interaction (Electrosorption and Evolution) Characteristics of Pd and Pd3Co Alloy Nanoparticles: An In-situ Investigation with Electrochemical Impedance Spectroscopy. *Electrochim. Acta* **2016**, *194*, 199−210.

(43) Navarro-Flores, E.; Chong, Z.; Omanovic, S. Characterization of Ni, NiMo, NiW and NiFe electroactive coatings as electrocatalysts for hydrogen evolution in an acidic medium. *J. Mol. Catal. A: Chem.* **2005**, *226* (2), 179−197.

(44) Strasser, P.; Koh, S.; Anniyev, T.; Greeley, J.; More, K.; Yu, C.; Liu, Z.; Kaya, S.; Nordlund, D.; Ogasawara, H.; Toney, M. F.; Nilsson, A. Lattice-strain control of the activity in dealloyed core-shell fuel cell catalysts. *Nat. Chem.* **2010**, *2* (6), 454−60.

(45) Yan, K.; Maark, T. A.; Khorshidi, A.; Sethuraman, V. A.; Peterson, A. A.; Guduru, P. R. The Influence of Elastic Strain on Catalytic Activity in the Hydrogen Evolution Reaction. *Angew. Chem., Int. Ed.* **2016**, *55* (21), 6175−81.

(46) Li, H.; Tsai, C.; Koh, A. L.; Cai, L.; Contryman, A. W.; Fragapane, A. H.; Zhao, J.; Han, H. S.; Manoharan, H. C.; Abild-Pedersen, F.; Nørskov, J. K.; Zheng, X. Activating and optimizing MoS$_2$ basal planes for hydrogen evolution through the formation of strained sulphur vacancies. *Nat. Mater.* **2016**, *15* (1), 48−53.

(47) Wang, L.; Zeng, Z.; Gao, W.; Maxson, T.; Raciti, D.; Giroux, M.; Pan, X.; Wang, C.; Greeley, J. Tunable intrinsic strain in two-dimensional transition metal electrocatalysts. *Science* **2019**, *363* (6429), 870−874.

(48) Ling, T.; Yan, D. Y.; Wang, H.; Jiao, Y.; Hu, Z.; Zheng, Y.; Zheng, L.; Mao, J.; Liu, H.; Du, X. W.; Jaroniec, M.; Qiao, S. Z. Activating cobalt(II) oxide nanorods for efficient electrocatalysis by strain engineering. *Nat. Commun.* **2017**, *8* (1), 1509.

(49) Sensoy, M. G.; Vinichenko, D.; Chen, W.; Friend, C. M.; Kaxiras, E. Strain effects on the behavior of isolated and paired sulfur vacancy defects in monolayer MoS$_2$. *Phys. Rev. B: Condens. Matter Mater. Phys.* **2017**, *95* (1), 014106.